Organic photovoltaic cells with nano-fabric heterojunction structure

June Hyoung Park,[1] Austin R. Carter,[1] Lynetta M. Mier,[2] Chi-Yueh Kao,[2] Sharlene A. M. Lewis,[2] Raju P. Nandyala,[1] Yong Min,[2,a)] and Arthur J. Epstein[1,2,a)]

[1]*Department of Physics, The Ohio State University, Columbus, Ohio 43210-1117, USA*
[2]*Department of Chemistry, The Ohio State University, Columbus, Ohio 43210-1173, USA*

Organic photovoltaic cells containing electron-transporting organic nanofibers in the form of "nanofabrics" are investigated. Nano-fabric heterojunctions of poly(3-hexylthiophene) and electron-transporting nanofibers significantly improve short-circuit current density in organic photovoltaic cells. The nanofibers and nanofabric are synthesized from organic electron-transporting material bis(octyl)-perylenediimide (PDI-C_8). The PDI-C_8 based nano-fabric's electron mobility is measured to be 0.08 cm^2/V s. The nanofabric improves charge collection by expanding the interfacial acceptor-donor area while simultaneously providing dedicated electron transport pathways to the LiF/Al electrodes. An increase in fill factor is observed for photovoltaic cells incorporating the nanofabric heterojunctions and is attributed to efficient removal of space charge. © *2012 American Institute of Physics*. [doi:10.1063/1.3679097]

Since the practical organic solar cell was reported in the 1980's, organic photovoltaic (OPV) cells have been studied as promising devices for energy production.[1] The discovery of fullerene and the developments of its soluble derivatives (e.g., 1-[3-(methoxycarbonyl)propyl]-1-phenyl-[6.6]C_{61} (PCBM)) led to a surge in their use as electron acceptors in OPV cells.[2–4] Fullerene's charge-transfer properties helped make the bulk heterojunction (BHJ) one of the most popular structures in current solid-state OPV cells.[5] But while short exciton diffusion lengths (~10 nm) in organic media necessitates small domains of donor and acceptor phases to separate charges, transport of those charges out of the cell relies on percolation pathways generated by larger features.[6,7] Structures with sizes comparable to the exciton diffusion length are perceived to optimize this trade-off and maximize cell efficiency. To satisfy this requirement, BHJ photovoltaic cells typically undergo thermal-annealing processes to create nanoclusters of donor and acceptor phases with characteristic sizes of ~20 nm.[8,9] However, reproducibly controlling nanomorphology through heat treatment is difficult. In addition, the segregated phases of PCBM in BHJ photovoltaic cells yield poorer electron mobility (10^{-3} to 10^{-6} cm^2/V s) than C_{60} prepared in poly-crystalline phase by thermal sublimation (~10^{-1} cm^2/V s).[10–12] Moreover, poor hole and electron mobilities (10^{-4} cm^2/V s) in BHJ photovoltaic blends results in high series resistances, which are not desirable for high short-circuit currents.[13–15] One dimensional structures such as nanofibers and nanorods are a potential solution to the problem of thermal stability and can provide dedicated pathways for transporting separated charges. Organic nano-structures such as fibers and fabrics have gained little attention as a means to improve performance of OPV devices.

Perylene diimide (PDI) materials have a long history in OPV cells[1] and cost significantly less than C_{60}-based materials. However, PDI materials have not garnered much attention in OPV due in part to the relative dominance of C_{60}-based materials.[5] Recently, many PDI-related materials

for OPV were synthesized and reviewed.[18–21] Xia and Bao *et al.*[22,23] have developed high electron mobility PDI materials and nanostructures as the active channel in organic transistors. This inspired us to develop PDI-based materials so that we may exploit their excellent electron transporting potential for OPV applications. We have developed a family of PDI materials[24] with different band gaps to modify absorption and a variety of nanostructures (e.g., nano-beads, nano-fibers, nano-networks) to enhance processability. Furthermore, we have incorporated these materials in a variety of configurations (e.g., nano-fabric heterojunction) to increase the acceptor-donor interactions needed for efficient charge separation. PDI can be used for collection of photo-generated electrons in OPV cells. Its electron mobility is as high as 0.1 cm^2/V s, which is comparable to that of pure fullerene films.[16] Due to strong π-stacking forces and an asymmetric molecular shape, PDI derivatives can form fibers with large aspect ratios. The diameters of the fibers can also be controlled by proper selection of functional groups bound to PDI core.[24] Exciton transfer length can be as long as a few microns; thus, PDI fibers are an excellent candidate for collection of photo-excited electrons.[25] In contrast to the poor solubility of PDI powder, PDI in nanofiber form enables solution processing to fabricate photovoltaic cells. The PDI absorption peaks range from 470 to 575 nm (Figure 1). Modification of perylene cores also can tune the electronic levels of the lowest unoccupied molecular orbit (LUMO) and highest occupied molecular orbit (HOMO) for optimal matching of donor-acceptor HOMO-LUMO levels.[16,17]

Bis(octyl)-perylenediimide (PDI-C_8, Figure 1(a)) was purchased from Sigma Aldrich Inc. and form PDI-C_8 nanofibers through self-assembly in a mixed solvent treatment of chloroform/methanol.[22] Fiber diameter is tunable between 10 nm and 1 μm based on solvent treatment.[24] The absorption spectra of PDI-C_8 feature multiple vibronic peaks, as shown in Figure 1(c). In the solution form of PDI-C_8 (methanol), the energy difference between HOMO and LUMO is approximately 2.39 eV (521 nm), while the energy difference in solid film is about 2.18 eV (567 nm). The absorption

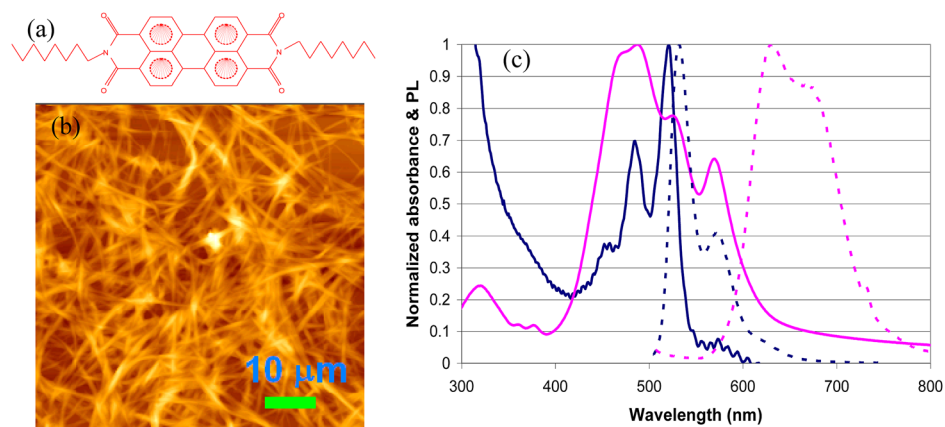a)Electronic addresses: epstein@mps.ohio-state.edu and yongm86@yahoo.com.

FIG. 1. (Color online) (a) Chemical structure of PDI-C8 molecule, (b) AFM image of isolated PDI-C8 nanofibers drop cast from solution, and (c) Optical absorbance (solid lines) and photoluminescence (dashed lines) of PDI-C8 solution in methanol (dark lines) and film (gray lines).

spectrum of PDI-C_8 nanofibers is similar to that of solid film of PDI-C_8 having a HOMO-LUMO gap of 2.16 eV (574 nm). The red-shift energy of the HOMO-LUMO gap from solution to solid forms of PDI-C_8 is relatively small, 0.21 eV. Fluorescence peaks of PDI-C_8 samples have a more pronounced red-shift from solution to solid phases by 0.36 eV. Thus, the aggregation energy in PDI-C_8 is approximately 0.15 eV, which is a relatively small value compared with other organic semiconductors. The field effect transistors mobility of PDI-C_8 thin films was measured to be 0.083 cm^2/V s, which indicates that PDI-C_8 will not limit mobility, and transport of separated electrons will be efficient.

For active layers in our photovoltaic cells, two kinds of solutions were prepared. One was a pure regio-regular P3HT solution, and the other was a mixture of PDI-C_8 nanofibers and regio-regular P3HT. Both solutions used HPLC grade o-dichlorobenzene as solvent. The concentration of the regio-regular P3HT (from Sigma-Aldrich Inc.) solution was about 1 wt. %, which was also used for the preparation of the mixture. To measure the weight of PDI-C_8 nanofibers, the dispersion of the nanofibers was initially vacuum-dried, and then, the net-weight of the nanofibers was measured. The nanofibers were not fused to each other even after a complete vacuum-dry process; thus, the nanofiber features were preserved in the mixed solution with P3HT. Weight ratio of P3HT to PDI-C_8 nanofibers was 5 or higher. Due to the light weight of PDI-C_8 nanofibers, we faced the limit of the resolution in our weighing scale. But we have confirmed the presence of nanofibers based on absorption spectra signature of PDI-C8 nanofibers in the active layers.

Our photovoltaic cells employed a semi-transparent copper anode (~13 nm) that was patterned by thermal evaporation on UV-ozone cleaned glass substrates. A hole-transporting layer (AI4083 PEDOT:PSS from Bayer) was subsequently applied by spin coating with an approximate thickness of 40 nm. The solutions for active layers were also spin-coated with an approximate thickness of 100 nm. The thicknesses of the spun layers were measured with an atomic force microscope from Pacific Nanotechnology Inc. Hole blocking PDI-C_8 film (20 nm) was thermally evaporated for some of our cells. Finally, LiF (0.5 nm) and aluminum (40 nm) layers were thermally evaporated to build electron-collecting electrodes for photovoltaic cells. No thermal annealing process was carried out throughout the fabrication. The thicknesses of the

single P3HT layer and the layer from the mixture of P3HT and PDI-C_8 nanofibers were 100 +/− 10 nm. Thus, the light absorptions by P3HT in both types of photovoltaic cells were similar. The amount of PDI-C_8 nanofibers was minimal, so we did not expect significant light absorption by the nanofibers. IV characteristic curves were obtained using an AM1.5G filtered solar simulator (Newport Oriel 96000) in a dry box to prevent the aging effects at LiF layers and P3HT layers. The illumination power was adjusted to be 100 mW/cm^2 using an optical powermeter (Coherent Power Meter Model 210).

As shown in Figure 2, four types of OPV cell structures and corresponded energy diagrams were constructed to investigate the role of PDI-C_8 nanofibers, which were classified by adding PDI-C_8 nanofibers and/or PDI-C8 electron collecting layer (hole blocking layer). Types I and III had active layers of pure P3HT, while types II and IV had active layers of the mixture. Types III and IV had a bi-layered heterojunction structure with an additional PDI-C_8 electron-collecting layer (hole-blocking layer), while types I and II were single-layered photovoltaic cells without any hole-blocking layer. In the comparison of the OPV's without hole blocking layers (types I and II), the embedded PDI-C_8
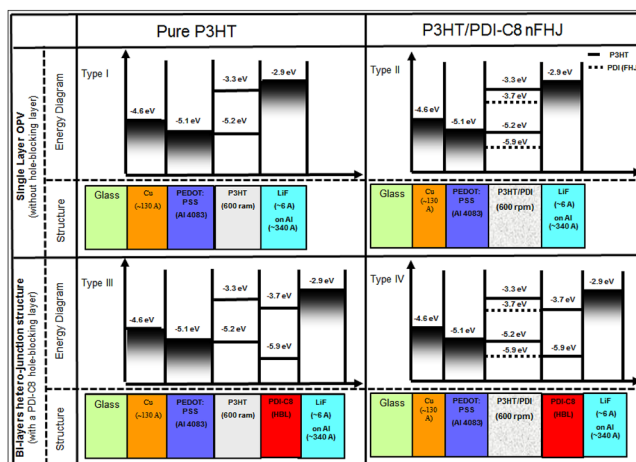

FIG. 2. (Color online) Four types of OPV cell structures and corresponded energy diagrams are constructed to investigate the role of PDI-C8 nanofibers, where types I and III have active layers of pure P3HT, while types II and IV have active layers of the mixture of P3HT and PDI-C8 nanofibers that form an nano-fabric heterojunction.

nanofibers did not improve the performance of OPV's (Figures 2(a) and 2(b)). During the mixing of P3HT and PDI-C$_8$ nanofibers, P3HT surrounded the nanofibers efficiently, which was observed in AFM phase-mode images (not shown). This makes PDI-C$_8$ nanofibers in the OPV's had a limited connecting area into LiF/Al electrodes. In fact, the efficiency in type II OPV was lower than that in type I due to lower open-circuit voltage, which implied that the work function of the electron collecting electrode (LiF/Al) was pinned to the LUMO of PDI-C$_8$ rather than that of P3HT.[26,27] This could also be seen by the open-circuit voltages in types III and IV OPV's, which was close to those in type II OPV's. Thus, PDI-C$_8$ nanofibers in type II did accept photo-excited electrons from P3HT absorbing material and fixed its open-circuit voltage. However, the efficiency of electron collection in type II was low due to the limited connection between PDI-C8 nanofibers and the LiF/Al electrode.

The addition of a thin electron-collecting PDI-C$_8$ layer into type III/IV OPV significantly improved short circuit currents (I$_{SC}$). Type III had more contact area between LiF/Al electrode and electron-collecting layer to ensure more photo-excited electron collection than type II. Moreover, another addition of PDI-C$_8$ nanofibers into light-absorbing P3HT layer of type III OPV, i.e., type IV OPV, significantly improved the efficiency by more than 100% (see Table I).[28] Thus, PDI-C$_8$ nanofibers significantly improved charge collection by extending the heterojunction area into the bulk and enhancing the transport of the separated electrons, which also included the electrons generated far away from the LiF/Al electrode. The nanofibers also improved the shape of IV characteristic curves (Figure 3). IV curves of type III show high differential resistance near open-circuit voltage (related to series resistance), which implied charge accumulation at the interface of the heterojunction (note that the interfaces at both electrodes were considered to be ohmic). In contrast to type III, type IV OPV's exhibit smaller series resistance. The charge mobility in type III OPV's is reduced to $\mu = 9 \times 10^{-4}$ cm^2/V s, which was calculated by using the formula about space-charge limited current[29]

$$J = \frac{9}{8}\varepsilon_r\varepsilon_0\mu\frac{(V - V_{bi})^2}{L^3}.\qquad(1)$$

Here, we used the open-circuit voltage of the device for a built-in potential (V_{bi}) and took a dielectric constant, $\varepsilon_r = 3$. The SCLC effective mobility in type III OPV is poorer than that in type IV by a factor of 3 due to the high internal resistance of the donor-acceptor planar architecture (see Table I).

TABLE I. Key parameters of four device configurations comparing the effect of PDI nanofibers on device performance.

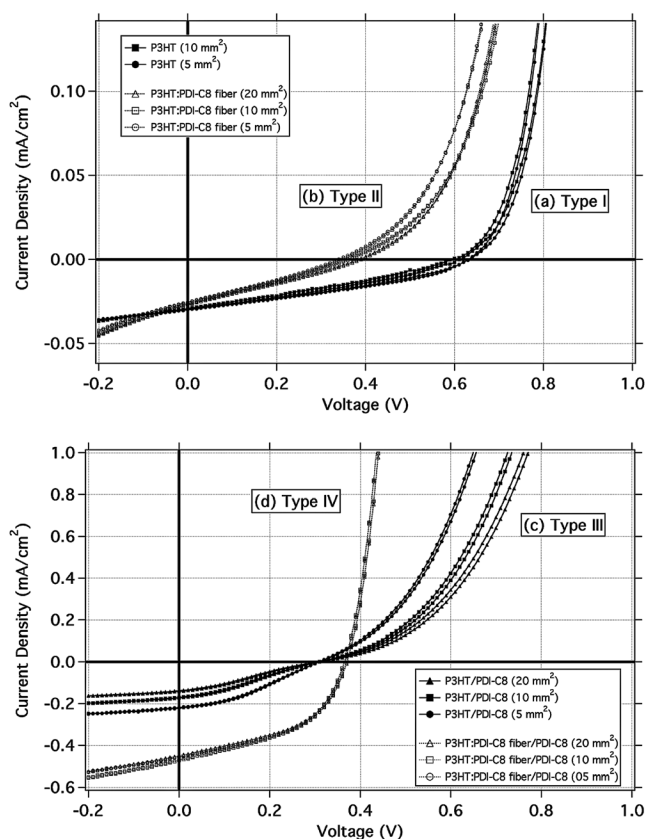| Device	μ (cm^2/V s)	V_{oc}	J_{sc} (mA/cm^2)	FF
P3HT:Al	7.1×10^{-4}	0.668	3.13×10^{-2}	0.005
Blend:Al	2.6×10^{-4}	0.331	2.65×10^{-2}	0.288
P3HT:BL:Al	9.0×10^{-5}	0.310	2.25×10^{-1}	0.348
Blend:BL:Al	3.1×10^{-4}	0.360	4.73×10^{-1}	0.482

FIG. 3. IV characteristic curves of the four device structures. Upper plot corresponds to types I and II OPV's and lower plot to types III and IV OPV's.

In summary, we have demonstrated the improvement of the short circuit current density of organic photovoltaic cells by implementing organic electron-transporting nanofibers forming nanofabric heterojunction. Bis(octyl)-perylenediimide is a good electron transporter based on the measurements of FET and forms nanofibers due to functional octyl groups on the perylenediimide core. The use of PDI-C$_8$ hole blocking layer facilitates electron collection, but the interface between the PDI-C$_8$ hole blocking layer and the absorbing P3HT layer likely increases series resistance, as observed in IV characteristic curves near open-circuit voltage. The use of PDI-C$_8$ nanofibers improves photovoltaic cells by (a) facilitating collection of photo-excited electrons in the P3HT bulk, (b) providing a dedicated transport pathway for electrons to the LiF/aluminum electrode, and (c) removal of accumulated photo-generated charges, which improves the fill factor.

[1] C. W. Tang, Appl. Phys. Lett. **48**, 183 (1986).
[2] H. W. Kroto, J. R. Heath, S. C. O'Brien, R. F. Curl, and R. E. Smalley, Nature (London) **318**, 162 (1985).
[3] J. C. Hummelen, B. W. Knight, F. LePeq, F. Wudl, J. Yao, and C. L. Wilkins, J. Org. Chem. **60**, 532 (1995).
[4] C. J. Brabec, F. Padinger, N. S. Sariciftci, and J. C. Hummelen, J. Appl. Phys. **85**, 6866 (1999).
[5] G. Yu, J. Gao, J. C. Hummelen, F. Wudl, and A. J. Heeger, Science **270**, 1789 (1995).
[6] J. J. M. Halls, K. Pichler, R. H. Friend, S. C. Moratti, and A. B. Holmes, Appl. Phys. Lett. **68**, 3120 (1996).
[7] P. Peumans, A. Yakimov, and S. R. Forrest, J. Appl. Phys. **93**, 3693 (2003).
[8] G. Dennler, M. C. Scharber, and C. J. Brabec, Adv. Mater. **21**, 1323 (2009).
[9] J. S. Moon, J. K. Lee, S. Cho, J. Byun, and A. J. Heeger, Nano Lett. **9**, 230 (2009).
[10] E. Frankevich, Y. Maruyama, and H. Ogata, Chem. Phys. Lett. **214**, 39 (1993).
[11] R. C. Haddon, A. S. Perel, R. C. Morris, T. T. M. Palstra, A. F. Hebard, and R. M. Fleming, Appl. Phys. Lett. **67**, 121 (1995).
[12] V. D. Mihailetchi, J. K. J. van Duren, P. W. M. Blom, J. C. Hummelen, R. A. J. Janssen, J. M. Kroon, M. T. Rispens, W. J. H. Verhees, and M. M. Wienk, Adv. Funct. Mater. **13**, 43 (2003).
[13] Z. Bao, A. Dodabalapur, and A. J. Lovinger, Appl. Phys. Lett. **69**, 4108 (1996).
[14] Y. Kim, S. Cook, S. M. Tuladhar, S. A. Choulis, J. Nelson, J. R. Durrant, D. D. C. Bradley, M. Giles, I. McCulloch, C.-S. Ha, and M. Ree, Nature Mater. **5**, 197 (2006).

[15] V. D. Mihailetchi, H. Xie, B. de Boer, L. J. A. Koster, and P. W. M. Blom, Adv. Funct. Mater. **16**, 699 (2006).
[16] R. Schmidt, M. M. Ling, J. H. Oh, M. Winkler, M. Konemann, Z. Bao, and F. Würthner, Adv. Mater. **19**, 3692 (2007).
[17] J. H. Oh, Y. S. Sun, R. Schmidt, M. F. Toney, D. Nordlund, M. Konemann, F. Würthner, and Z. N. Bao, Chem. Mater. **21**, 5508 (2009).
[18] C. Li, M. Y. Liu, N.G. Pschirer, M. Baumgarten, and K. Müllen, Chem. Rev. **110**, 6817 (2010).
[19] A. Tolkki, E. Vuorimaa, V. Chukharev, H. Lemmetyinen, P. Ihalainen, J. Peltonen, V. Dehm, and F. Würthner, Langmuir **26**, 6630 (2010).
[20] S. Ko, R. Mondal, C. Risko, J. K. Lee, S. Hong, M. D. McGehee, J.-L. Brédas, and Z. Bao, Macromolecules **43**, 6685 (2010).
[21] Y. P. Yi, V. Coropceanu, and J.-L. Brédas, J. Mater. Chem. **21**, 1479 (2011).
[22] A. L. Briseno, S. C. B. Mannsfeld, C. Reese, J. M. Hancock, Y. Xiong, S. A. Jenekhe, Z. Bao, and Y. Xia, Nano Lett. **7**, 2847 (2007).
[23] A. L. Briseno, S. C. B. Mannsfeld, S. A. Jenekhe, Z. Bao, and Y. Xia, Mater. Today **11**, 38 (2008).
[24] A. J. Epstein and Y. Min, U.S. Provisional Patent No. 61/391,436 (8 October 2010).
[25] B. A. Gregg, J. Sprague, and M. W. Peterson, J. Phys. Chem. B **101**, 5362 (1997).
[26] V. D. Mihailetchi, P. W. M. Blom, J. C. Hummelen, and M. T. Rispens, J. Appl. Phys. **94**, 6849 (2003).
[27] C. J. Brabec, A. Cravino, D. Meissner, N. S. Sariciftci, T. Fromherz, M. T. Rispens, L. Sanchez, and J. C. Hummelen, Adv. Funct. Mater. **11**, 374 (2001).
[28] R. H. Parmenter and W. Ruppel, J. Appl. Phys. **30**, 1548 (1959).
[29] M. A. Lampert and P. Mark, *Current Injection in Solids* (Academic Press, New York, 1970).